Printed in the Republic of Korea

ANALYTICAL SCIENCE & TECHNOLOGY

Vol. 31 No. 1, 1-6, 2018

https://doi.org/10.5806/AST.2018.31.1.1

Nanoconfinement effects of MCM-41 on the thermal decomposition of metal borohydrides

Sanghoon Kim, Hyejin Song, and Chul Kim★

Department of Chemistry, Hannam University, Daejeon 34054, Korea

(Received October 26, 2017; Accepted December 26, 2017)

Abstract We used differential scanning calorimetry and a thermogravimetric analysis to investigate the effect of being confined in mesoporous MCM-41 on the decomposition of lithium borohydride and magnesium borohydride when heated. The confinement did not cause a phase transition of the metal borohydrides inside MCM-41, but did lower their decomposition temperature. With the exception of a lowering of the temperature, the decomposition reaction mechanism of the metal borohydrides was nearly the same for both the bulk and confined samples.

Key words: Hydrogen storage, Dehydrogenation, Lithium borohydride $LiBH_4$, Magnesium borohydride $Mg(BH_4)_2$, MCM-41

1. Introduction

Metal borohydrides, such as $LiBH_4$, $Mg(BH_4)_2$, and $Ca(BH_4)_2$, are promising hydrogen storage materials that have high gravimetric and volumetric hydrogen densities, of 18.5 wt%, 14.9 wt%, and 11.5 wt%, respectively.[1-4]

Although the hydrogen contents of these materials are very high, the kinetics and thermodynamics of the hydrogen desorption and absorption suffer from the very high temperature needed for these reactions.[5,6]

Many remarkable improvements in the kinetics and thermodynamics have been achieved by using catalysts such as nanosized Ni,[7] Al metal,[8] and $TiCl_4$,[9] or nanoconfinement in meso- or microporous materials, such as carbon aerogels, mesoporous silica scaffolds, and activated carbon, with nanopores of 7-25 nm, 1.51-10 nm, and < 4 nm in diameter, respectively.[10-12]

Mesoporous silica materials have been used to confine the hydrogen storage materials in order to improve their properties by, for example, suppressing side products, modifying the desorption enthalpy, and lowering the activation barrier for the loss of H_2.[13]

Some studies on why the kinetics and thermodynamics are improved in nanoconfined metal borohydrides showed interesting effects of fluidic $LiBH_4$ on the scaffold surfaces, and proposed a confinement mechanism under the surface effect of mesoporous materials.[1,14]

The mesoporous material MCM-41 has negligible

★ Corresponding author
Phone : +82-(0)42-629-8875 Fax : +82-(0)42-629-8811
E-mail : chulkim@hnu.kr

catalytic activity, because of its framework neutrality, but does have advantageous properties, such as good thermal conductivity, high surface area, and retention of surface area at high temperature. MCM-41 has been used to increase the conductivity of Li^+ as a solid electrolyte by confining $LiBH_4$ in the mesoporous silica scaffold.[15,16]

Here, we used MCM-41 to confine the metal borohydrides in the nanopores formed in the well-ordered channels of MCM-41 in order to improve its hydrogen desorption.

In this study, we used differential scanning calorimetry (DSC) and thermogravimetric analysis (TGA) to investigate how the thermodynamics of metal borohydrides are improved by being confined inside the MCM-41. We found that confining metal borohydrides inside MCM-14 is very promising as a way to improve the hydrogen desorption of these borohydrides.

2. Experimental

Metal borohydrides, MCM-41, and tetrahydrofuran (THF) were purchased from Aldrich and used without any treatment. Freeze-thawing was applied to the THF solvent in a vacuum manifold in order to remove oxygen and water in the solvent. MCM-41 was heated for 5 hours at 250 °C in the vacuum manifold to remove impurities. Wet infiltration of metal borohydrides into the MCM-41 was performed using the method of Fang *et al*.[17]

Lithium borohydride was put into the THF solvent, to which MCM-41 was added. The mixed solution was put in the vacuum manifold and heated for 72 hours to remove water and THF solvent, during which the lithium borohydride was infiltrated into the nanopores of MCM-41.

We used a Micromeritics ASAP 2000 to analyze the extent of lithium borohydride infiltration using the Brunauer-Emmett-Teller (BET) method. The pressure of nitrogen gas was changed from 8 to 780 mmHg. The total volume was evaluated from the adsorbed amount of gas at the relative pressure of 0.99. Pore-size distributions of MCM-41 were derived by using the Barret-Joyner-Halenda (BJH) calculation to analyze the adsorption branch.[18]

Scinco DSC N-650 and Scinco TGA N-1000 were used for the differential scanning calorimetry and for the thermal gravimetric analysis, respectively. The samples, sealed into an aluminum pan with a lid, were heated up to 600 °C at ramping rates of 20 °C/min and 4.6 °C/min for DSC and TGA, respectively.

3. Results and Discussion

3.1. Nanoconfinement of $LiBH_4$ and $Mg(BH_4)_2$ inside MCM-41

The BET curve in *Fig.* 1(a) shows that the mesoporous material MCM-41 is a type IV as classified by IUPAC.[19]

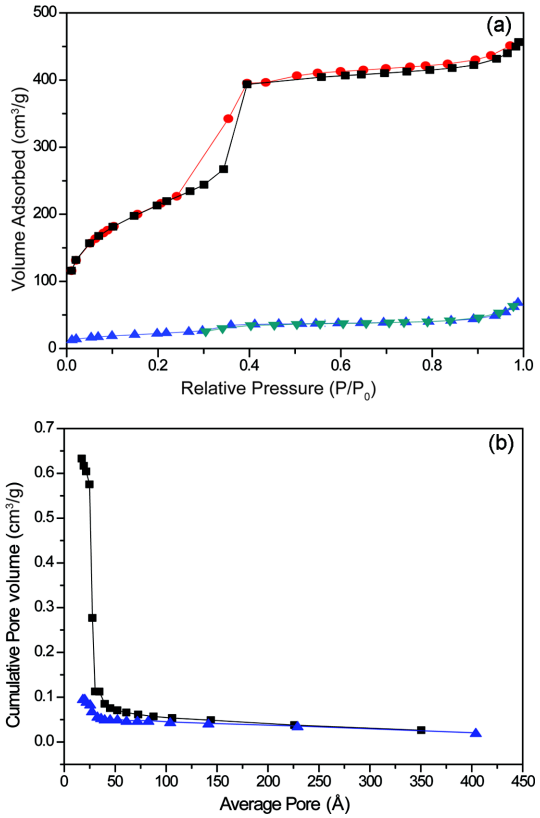

Fig. 1. (a) N_2 adsorption/desorption BET isotherms and (b) BJH pore size distribution curves of pure MCM-41 (circle and rectangle) and $LiBH_4$-infiltrated MCM-41 (triangle).

One characteristic feature is the initial part of the isotherm, which is attributed to monolayer-multilayer adsorption shown in general adsorption in a nonporous form. The second one is a hysteresis loop, which may result from the capillary condensation in mesopores. The third one is the limiting uptake over a high relative pressure.[20]

As is shown in *Fig.* 1(b), about 80% of pores with a diameter of less than 5 nm in pure MCM-41 were reduced by the infiltration of $LiBH_4$. When the number of pores in pure MCM-41 was calculated from the data shown in *Fig*. 1(b), most pores had diameters of 2.5 to 2.8 nm; hence the pores of the MCM-41 used in this experiment were about 2.7 nm on average. Counting only pores of that size, 97% of the mesopores in MCM-41 were filled with $LiBH_4$; hence wet filtration efficiently infiltrates the metal borohydrides into the nanopores in MCM-41.

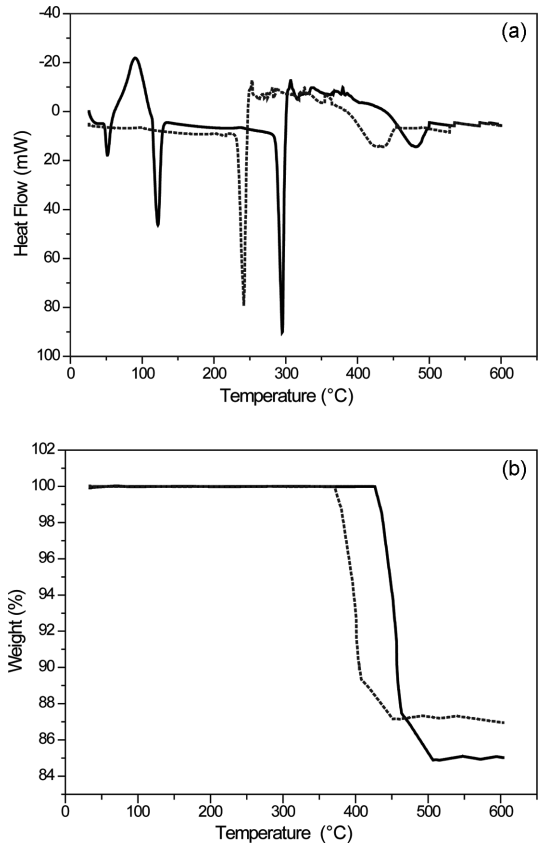

Fig. 2. (a) DSC and (b) TGA profiles of bulk $LiBH_4$ (solid curve) and nanoconfined $LiBH_4$ (dotted curve).

3.2. Thermal decomposition of bulk $LiBH_4$ and nanoconfined $LiBH_4$

The DSC profile of bulk $LiBH_4$ in *Fig.* 2(a) shows two sharp and one broad endothermic peak (sold curve). The first sharp peak at 122 °C arises from a structural transition from the orthorhombic low-temperature (LT) phase to the hexagonal high-temperature (HT) phase. This temperature is a little higher than the 108-112 °C reported in another paper.[21]

This difference seemed to be caused by the difference in experimental conditions. The second peak, at 295 °C, corresponds to melting of the bulk $LiBH_4$ powder, which agrees well with the TGA result (solid curve), which shows no weight loss at this temperature. The broad peak starting at 427 °C and ending at 507 °C reveals the thermal decomposition of the bulk $LiBH_4$. The maximum decomposition rate occurred at 481 °C. The TGA result also shows the weight loss of the sample induced by the generation of hydrogen gas in this temperature range. The TGA curve also shows that hydrogen release started at 427 °C and ended at 507 °C. The decomposition reaction is as follows:[22]

$$LiBH_4 \rightarrow LiH + B + 3/2H_2 \quad (1)$$

The DSC profile of the $LiBH_4$ nanoconfined inside MCM-41 shows one sharp and one broad endothermic peak (dotted curve). The sharp peak at 243 °C seems to correspond to the melting of $LiBH_4$ inside the MCM-41. The broad peak starting at 372 °C and ending at 450 °C may reveal the thermal decomposition of $LiBH_4$ confined inside the MCM-41. The maximum decomposition rate occurred at 431 °C. This value is similar to the decomposition temperature of 375 °C of $LiBH_4$ confined in active carbon.[11]

The decomposition at this temperature agrees well with the TGA results, which show the weight loss of the sample in this temperature range. The TGA curve shows that hydrogen release started at 372 °C and ended at 450 °C (dotted curve). There is no peak at around 120 °C, at which the LT phase of the bulk $LiBH_4$ changes to the HT phase; so there is no phase transition of $LiBH_4$ confined inside MCM-41. It is

not clear yet why there is no such change.

The results shown in *Fig.* 2 indicate that the melting temperature of the nanoconfined $LiBH_4$ was lowered by 52 °C by the nanoconfinement effect. The decomposition temperature was also lowered by 50 °C, a value very similar to the lowering of the melting temperature. It is not clear yet why the degrees of the nanoconfinement effect are the same for both melting and decomposition.

Decomposed hydrogen was 15 wt% for the bulk $LiBH_4$ and 13 wt% for the nanoconfined $LiBH_4$. *Table* 1 shows the experimental results.

3.3. Thermal decomposition of bulk $Mg(BH_4)_2$ and nanoconfined $Mg(BH_4)_2$

Results similar to those for $LiBH_4$ were obtained for $Mg(BH_4)_2$. The decomposition temperature was lowered for the $Mg(BH_4)_2$ confined inside MCM-41, but more than it was for $LiBH_4$.

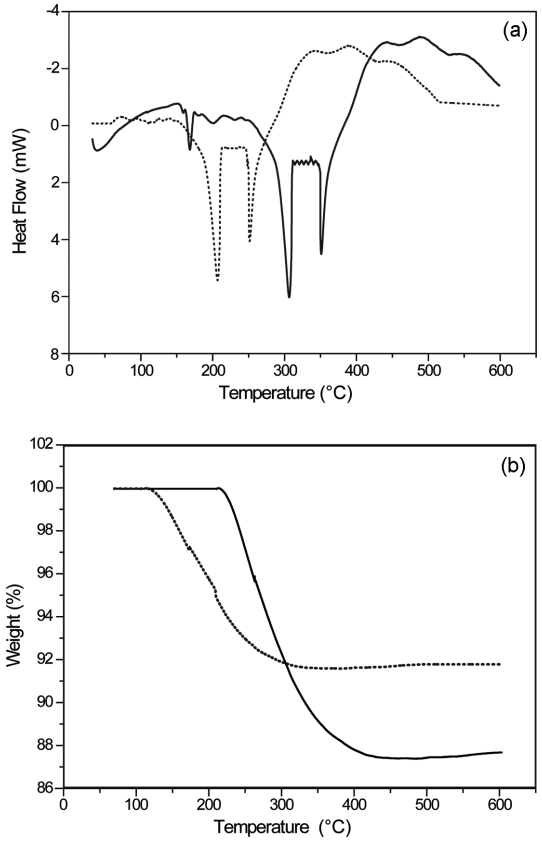

Fig. 3. (a) DSC and (b) TGA profiles of bulk $Mg(BH_4)_2$ (solid curve) and nanoconfined $Mg(BH_4)_2$ (dotted curve).

The DSC profile of bulk $Mg(BH_4)_2$ in *Fig.* 3(a) shows three sharp endothermic peaks and one broad exothermic peak (solid curve). The small, sharp peak at 168 °C corresponds to a structural transition from the LT phase to the HT phase. This temperature is little lower than the 184 °C reported in another paper,[2] probably because of the difference in experimental conditions. The second and third peaks, at 306 °C and 351 °C, can be assigned to the decomposition of magnesium borohydride to magnesium hydride and boron and then to magnesium metal (Eqs. (2) and (3)).[2]

$$Mg(BH_4)_2 \rightarrow MgH_2 + 2B + 3H_2 \quad (2)$$

$$MgH_2 \rightarrow Mg + H_2 \quad (3)$$

TGA measurement shows a curve consistent with the DSC result, that hydrogen release started at 215 °C and ended at 430 °C. The broad exothermic peak starting at 380 °C may be assigned to the formation of MgB_2,[2] but TGA did not show any further weight loss caused by the release of hydrogen gas in this temperature range. This remains unexplained.

The DSC profile of $Mg(BH_4)_2$ confined inside MCM-41 shows two sharp endothermic peaks and one broad exothermic peak (dotted curve). There is no peak at around 168 °C, so the phase transition of magnesium borohydride did not occur inside MCM-41. The first and second peaks, at 206 °C and 251 °C, can be assigned to the decomposition of magnesium borohydride to magnesium hydride and boron (Eq. (2)). TGA measurement also shows a curve consistent with the DSC result that hydrogen release started at 115 °C and ended at 330 °C. The broad exothermic peak starting at 282 °C may be assigned to the formation of MgB_2,[2] but TGA did not show any further weight loss caused by the release of hydrogen gas. This remains unexplained.

The results shown in *Fig.* 3 indicate that the decomposition temperature was lowered by 100 °C, which is more than the temperature lowering for $LiBH_4$ confined inside MCM-41. Decomposed hydrogen was 12.7 wt% for the bulk $Mg(BH_4)_2$ and

Table 1. Summary of DSC and TGA results for $LiBH_4$ and $Mg(BH_4)_2$

Metal hydrides	Crystal conversion temperature (°C)	Melting temperature (°C)	Decomposition temperature (°C)	Decomposed hydrogen (wt%)
Bulk $LiBH_4$	122	295	481 (427-507)[a]	(15.0)
Nanoconfined $LiBH_4$		243	431 (372-450)	(13.0)
Bulk $Mg(BH_4)_2$	168		306, 351, 380-600 (215-430)	(12.7)
Nanoconfined $Mg(BH_4)_2$			206, 251, 282-515 (115-330)	(8.3)

[a]TGA data in parenthesis

8.3 wt% for the nanoconfined $Mg(BH_4)_2$. *Table* 1 shows all the experimental results.

3.4. Temperature lowering effect of MCM-41 on decomposition of $LiBH_4$ and $Mg(BH_4)_2$

The effects of nanoconfinement on the decomposition of metal borohydrides can be classified into three parts: size effects, confinement effects, and support effects. Size effects are related to the increase in the surface energy that stabilizes or destabilizes metal borohydrides. Confinement leads to both kinetic and thermodynamic effects. Physical confinement may restrict the phase segregation of the dehydrogenated products from the metal borohydrides by affecting the desorption and absorption of hydrogen. Confinement also restricts the volume change following the absorption/desorption reaction, which changes the reaction enthalpies from those of the bulk metal borohydrides. Support effects are the physical, chemical, and electronic interactions of the metal borohydrides with the nanoporous host materials.

The temperature lowered differently for the lithium borohydride and magnesium borohydride, perhaps because the chemical and electronic interactions between the nanopores of MCM-41 and lithium borohydride differ from those between the nanopores of MCM-41 and magnesium borohydride. However, the size and confinement effects of MCM-41 may not induce this difference, because the physical and geometrical situations inside nanopores in both cases are nearly the same.

4. Conclusions

Nanoconfinement of metal borohydrides in the mesopores of MCM-41 affects their melting temperature and the decomposition temperature. Decomposition temperature was lowered by 50 °C and 100 °C for lithium borohydride and magnesium borohydride, respectively. Nanoconfinement prevents the phase transition of the nanoconfined metal borohydrides. The similarity of the DSC curves for both the bulk metal hydrides and the nanoconfined metal hydrides indicates that the reaction mechanisms of the nanoconfined metal borohydrides may be same as those of the bulk ones.

Acknowledgements

This work was supported by the Basic Science Research Program through the National Research Foundation of Korea (NRF) funded by the Ministry of Education (NRF-2017R1D1A3B04033122).

References

1. H. S. Lee, S. J. Hwang, M. To, Y. S. Lee, and Y. W. Cho, *J. Phys. Chem. C,* **119**(17), 9025-9035 (2015).
2. G. L. Soloveichik, Y. Gao, J. Rijssenbeek, M. Andrus, S. Kniajanski, R. C. Bowman, S. J. Hwan, and J. C. Zhao, *Int. J. Hydrog. Energy,* **34**(2), 916-928(2009).
3. O. Zavorotynska, A. El-Kharbachi, S. Deledda, and B. C. Hauback, *Int. J. Hydrog. Energy,* **41**(32), 14387-14403 (2016).
4. C. Bonatto Minella, E. Pellicer, E. Rossinyol, F. Karimi, C. Pistidda, S. Garroni, C. Milanese, P. Nolis, M. D. Baró, O. Gutfleisch, K. P. Pranzas, A. Schreyer, T. Klassen, R. Bormann, and M. Dornheim, *The J. Phys. Chem. C,* **117**(9), 4394-4403 (2013).
5. J. Vajo John, L. Skeith Sky, and F. Mertens, *The J. Phys.*

Chem. B, **109**(9), 3719-22 (2005).
6. K. Chlopek, C. Frommen, A. Leon, O. Zabara, and M. Fichtner, *J. Mater. Chem.,* **17**(33), 3496-3503 (2007).
7. H. W. Li, Y. Yan, E. Akiba, and S. I. Orimo, *Mater. Trans.,* **55**(8), 1134-1137 (2014).
8. Y. J. Choi, J. Lu, H. Y. Sohn, Z. Z. Fang, C. Kim, R. C. Bowman, and S. J. Hwang, *J. Phys. Chem. C,* **115**(13), 6048-6056 (2011).
9. R. Gosalawit-Utke, C. Milanese, P. Javadian, A. Girella, D. Laipple, J. Puszkiel, A. S. Cattaneo, C. Ferrara, J. Wittayakhun, J. Skibsted, T. R. Jensen, A. Marini, T. Klassen, and M. Dornheim, *J. Alloys and Comp.,* **599**, 78-86 (2014).
10. T. K. Nielsen, U. Bösenberg, R. Gosalawit, M. Dornheim, Y. Cerenius, F. Besenbacher, and T. R. Jensen, *ACS Nano,* **4**(7), 3903-3908 (2010).
11. A. F. Gross, J. J. Vajo, S. L. Van Atta, and G. L. Olson, *The J. Phys. Chem. C,* **112**(14), 5651-5657 (2008).
12. T. K. Nielsen, F. Besenbacher, and T. R. Jensen, *Nanoscale,* **3**(5), 2086-2098 (2011).
13. A. Gutowska, L. Li, Y. Shin, C. M. Wang, X. S. Li, J. C. Linehan, R. S. Smith, B. D. Kay, B. Schmid, W. Shaw, M. Gutowski, and T. Autrey, *Angewandte Chemie - Inter. Edition,* **44**(23), 3578-3582 (2005).
14. S. J. Hwang, H. S. Lee, M. To, Y. S. Lee, Y. W. Cho, H. Choi, and C. Kim, *J. Alloys and Comp.,* **645**(S1), S316-S319 (2015).
15. S. Das, P. Ngene, P. Norby, T. Vegge, P. E. De Jongh, and D. Blanchard, *J. Electroch. Soc.,* **163**(9), A2029-A2034 (2016).
16. D. Blanchard, A. Nale, D. Sveinbjörnsson, T. M. Eggenhuisen, M. H. W. Verkuijlen, Suwarno, T. Vegge, A. P. M. Kentgens, and P. E. De Jongh, *Adv. Funct. Mate.,* **25**(2), 184-192 (2015).
17. Z. Z. Fang, P. Wang, T. E. Rufford, X. D. Kang, G. Q. Lu, and H. M. Cheng, *Acta Mater.,* **56**(20), 6257-6263 (2008).
18. E. P. Barrett, L. G. Joyner, and P. P. Halenda, *J. Am. Chem. Soc.,* **73**(1), 373-380 (1951).
19. Z. A. ALOthman, *Materials,* **5**, 2874-2902 (2012).
20. K. S. W. Sing, D. H. Everett, R. A. W. Haul, L. Moscou, R. A. Pierotti, J. Rouquerol, and T. Siemieniewska, *Pure and Applied Chem.,* **57**, 603-619 (1985).
21. S. Cahen, J. B. Eymery, R. Janot, and J. M. Tarascon, *J. Power Sour.,* **189**(2), 902-908(2009).
22. A. Züttel, P. Wenger, S. Rentsch, P. Sudan, P. Mauron, and C. Emmenegger, *J. Power Sour.,* **118**(1-2), 1-7 (2003).